ACS APPLIED MATERIALS & INTERFACES

www.acsami.org

Research Article

Polarization of Stem Cells Directed by Magnetic Field-Manipulated Supramolecular Polymeric Nanofibers

Bing Zhang, Qilin Yu, and Yu Liu*

Cite This: https://dx.doi.org/10.1021/acsami.0c19428

Read Online

ACCESS | Metrics & More | Article Recommendations | Supporting Information

ABSTRACT: Precise assembly of the cytoskeleton (*e.g.*, actin, tubulin, and intermediate filaments) is of great importance for stem cell polarization and tissue regeneration. Recently, artificial manipulation of cytoskeleton assembly for remodeling stem cell polarization and ultimate cell fates attracts more and more interest of both chemists and biologists. Herein, we report the magnetic field-directed formation of biocompatible supramolecular polymeric nanofibers composed of two subunits: a β-cyclodextrin-bearing hyaluronic acid host polymer (HACD) and magnetic nanoparticles modified with actin-binding peptide and adamantane (MS-ABPAda). Transmission electron microscopy indicated that when HACD and MS-ABPAda were exposed to a magnetic field, they self-assembled into long nanofibers along the direction of the magnetic field, and the rate of nanofiber formation was linearly correlated with the strength of the magnetic field. Interestingly, when incubated with dental pulp stem cells, the nanofibers specifically drove tip extension and polarization of the cells, a phenomenon that can be attributed to targeting of actin-binding peptide to the actin cytoskeleton and subsequent polarization of the nanofibers. The successful application of these magnetic field-responsive supramolecular polymers on accurately driving polarization of mammalian cells is expected to be of great value for artificially manipulating cell fate and developing intelligent responsive materials in regenerative medicine.

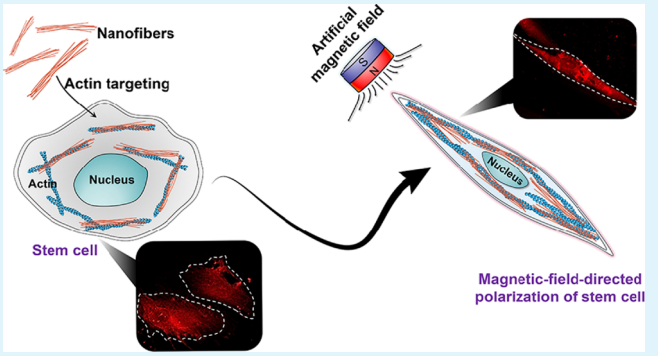

KEYWORDS: *actin cytoskeleton, cell polarization, cyclodextrin, self-assembly, supramolecular nanofiber*

1. INTRODUCTION

Cell polarization is an asymmetric cellular behavior with structural and functional change in lifecycles of all types of mammalian cells. Apart from a transient polarization process under exterior stimuli, permanent polarization process is also a common phenomenon, which directs destined fates of some kinds of cells (*e.g.*, epithelia, neurons, and odontoblasts).[1,2] At the tissue level, cell polarization is critical for many biological processes, such as embryonic development, tissue differentiation and regeneration, and neuron migration.[2−4] In mammalian cells, polarization is controlled by complicated networks of biological processes, *e.g.*, asymmetric distribution of cytoskeleton and repositioning of polarization-related proteins.[5−7] Recently, artificial regulation of cell polarization has received a surge of interest since it is of great importance for modulating regenerated tissues and organs.[8,9] Emerging studies have showed the potential of biomaterials to modulate cell behaviors, including cell polarization, cell migration, and so on.

Cellular polarization is known to be controlled by the rearrangement of the cytoskeleton. In particular, actin cytoskeleton, together with microtubules and intermediate filaments, plays a vital role in determination of polarization sites and polarized extension of cells.[10−12] In polarized epithelia, actin filaments usually perform an ordered arrangement relative to the tissue axis and subsequently propagate some specific cues to the related signaling proteins for the establishment of polarization.[1,10] Thus, developing biomaterials with the function of directing actin arrangement is an attractive approach to control cellular polarization and differentiation. Excellent actin-binding molecules, which provide the binding sites and traction possibility, are the core of a biomaterial design. Recently, the researchers found that the short peptide (named as "actin binding peptide", ABP), a *Saccharomyces cerevisiae*-derived peptide containing 17 amino acids (MGVADLIKKFESISKEE), could be efficiently used for targeting the filamentous actin (F-actin) in eukaryotic cells.[13,14] Therefore, the development of nanomaterials

Received: October 30, 2020
Accepted: February 11, 2021

Scheme 1. Schematic Illustration of the Formation of MS-ABPAda⊂HACD Nanofibers for Regulating cell Polarization. (a) Formation of MS-ABPAda⊂HACD Nanofibers Driven by host−Guest Interactions and (b) Magnetic Field-Directed Polarization of a Stem Cell.

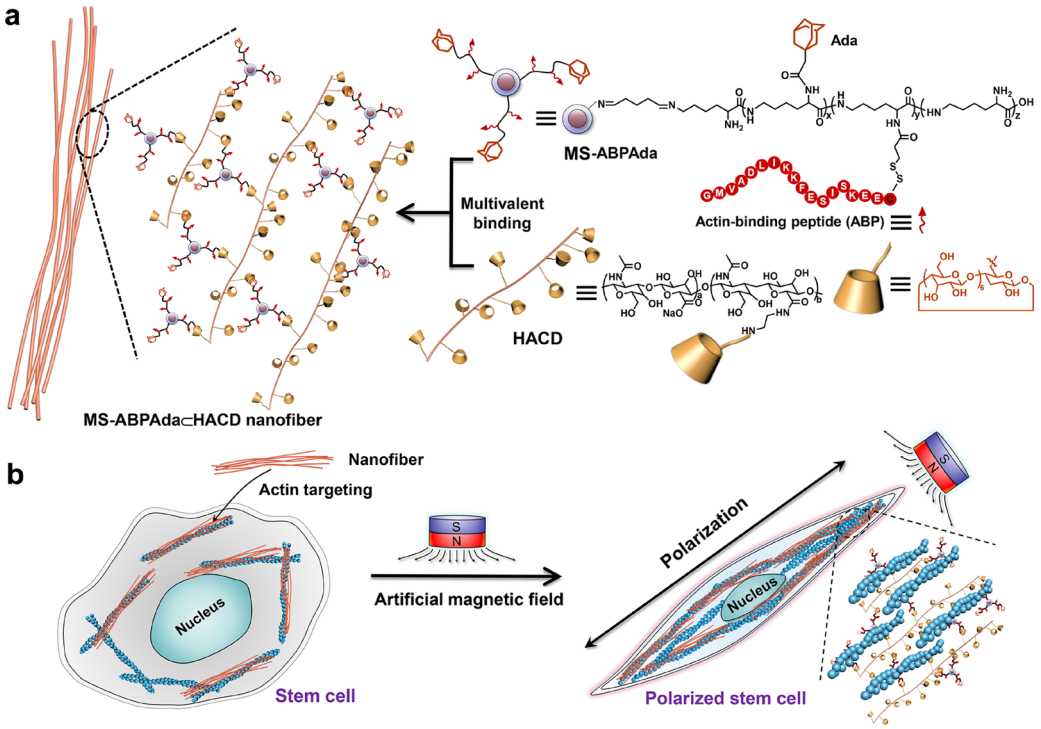

modified by ABP provides a new opportunity for regulation of actin arrangement and related cell behaviors.

Nanofiber materials constructed from supramolecular polymers composed of macrocyclic monomers have recently become the focus of a growing number of studies as a result of the rapid development of modern methods in chemistry, biology, and materials science.[15−18] Supramolecular polymers composed of supramolecules (*e.g.*, *β*-cyclodextrin (*β*-CD), cucurbituril, and pillararene) are of particular interest because these monomers show excellent biocompatibility, synthesize easily, and self-assemble readily.[19−21] The self-assembly of *β*-CD-based supramolecular polymers in aqueous solution is driven mainly by multiple noncovalent interactions between the *β*-CD host molecules and hydrophobic guest molecules such as adamantane (Ada), azobenzene, and ferrocene.[22−24] Biomimetic nanofibers consisting of CD-bearing long-chain biocompatible polymers (*e.g.*, polyethylene glycol, polylactic acid, hyaluronic acid [HA], and chitosan) have been extensively studied and used for a number of biomedical applications, such as suppression of tumor metastasis,[25−27] targeted drug delivery,[28−31] and inhibition of pathogenic infections.[32−34]

The effective artificial regulation of cell polarization requires stable interaction between the biomaterials and the intracellular element (such as filamentous actin) and the responsive dynamic manipulation. The external control of organelle−biomaterial interactions has been largely demonstrated by the use of photoirradiation, changes of pH, and application of a magnetic field.[25,35−37] Magnetic field is especially attractive on account of its advantages of being noninvasive, penetrative, and easy to control.[38,39] Taking advantage of these properties, Bian and his co-workers successfully regulated the adhesion and polarization of macrophages with RGD-bearing superparamagnetic nanoparticles (NPs) under the oscillating magnetic field.[40] Coincidentally, Gueroui et al. realized the spatiotemporal control of microtubule nucleation and assembly using magnetic nanoparticles under the static magnetic field.[41] Fan et al. developed heterovalency magnetic DNA nanoclaws with octopus arms morphology for synergetic cell capture.[42] Recently, our group reported the geomagnetic field-induced formation of AuNR-MitP-MNP⊂HACD nanofibers (NR, nanorod; MitP, mitochondrial targeting peptide; MNP, magnetic NPs), which display high photothermal efficiency and induce severe mitochondrial damage upon near-infrared irradiation.[43] These results indicate that magnetic field-controlled supramolecular assemblies have a great application potential in cell behavior regulation.

Of the various cell types found in mammalian organisms, dental pulp stem cells and neurons experience the frequent active polarized extension over their lifetimes and are considered as the desired cell experiment model for cell polarization research.[44,45] Herein, we report that the cross-linked supramolecular polymeric nanofibers can regulate the polarization of stem cells upon application of an artificial magnetic field. The nanofibers consist of two components: a *β*-CD-bearing HA polymer (HACD) and magnetic silica nanoparticles (MS) modified with actin-binding peptide (ABP) and Ada (Scheme 1a). Owing to host−guest interactions between the *β*-CDs and Ada and the presence of the magnetic NPs, the two components self-assembled strictly along the direction of the magnetic field. When incubated with stem cells under the magnetic field, the nanofibers promoted tip polarization and unidirectional extension of the cells which in turn led to cell polarization along the direction of the magnetic field (Scheme 1b). Our findings suggest that this is a promising chemical strategy for artificially regulating cellular

https://dx.doi.org/10.1021/acsami.0c19428
ACS Appl. Mater. Interfaces XXXX, XXX, XXX−XXX

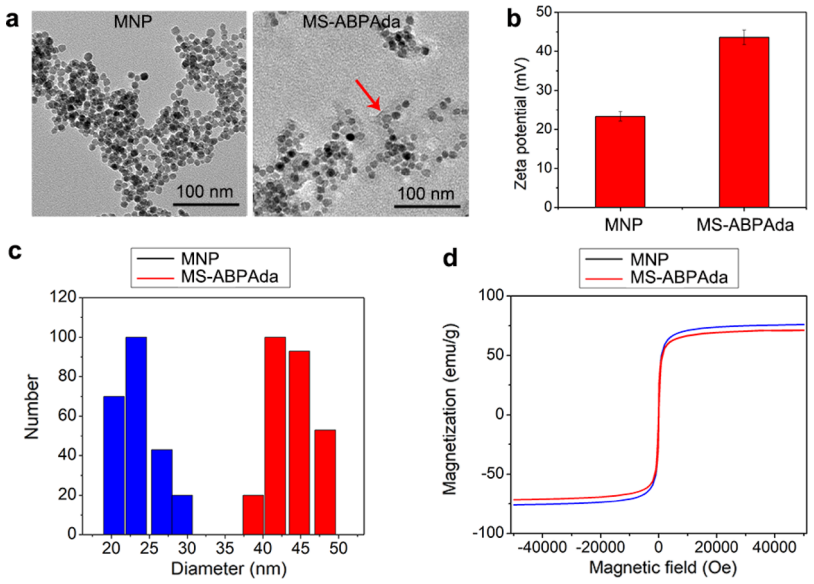

Figure 1. Characterization of the Fe_3O_4 and MS-ABPAda NPs. (a) TEM images, (b) zeta potentials, (c) size distributions (determined by dynamic light scattering analysis), and (d) magnetization curves of the NPs.

behaviors and may facilitate the development of supramolecular systems with applications in regenerative medicine.

2. RESULTS AND DISCUSSION

2.1. Material Design and Characterizations. The fabrication of the MS-ABPAda⊂HACD nanofibers is shown schematically in Figure S1. First, Fe_3O_4 NPs were synthesized by means of a co-precipitation method. Transmission electron microscopy (TEM) showed that the obtained NPs were spherical with diameters of 15−20 nm (Figure 1a), and X-ray diffraction analysis indicated that they were pure Fe_3O_4 (Figure S2). Treatment of these NPs with tetraethyl orthosilicate and then with aminopropyltriethoxysilane generated Fe_3O_4 NPs with modifiable amino groups on the surface (MS). The MS NPs were covalently modified with polylysine (plys, M_w = 5000), with mediation by glutaraldehyde, to afford MS-plys. Ada groups were grafted to some of the amino groups of MS-plys by means of the 1-ethyl-3-(3-dimethylaminopropyl) carbodiimide/*N*-hydroxysulfosuccinimide reaction, which afforded MS-plys-Ada. The resulting Ada-modified NPs were treated with ABP (FITC-ACP-MGVADLIKKFESISKEEC, where FITC = fluorescein isothiocyanate and ACP = aminocaproic acid) and *N*-succinimidyl-3-(2-pyridyldithio) propionate to generate actin-targeting magnetic NPs designated MS-ABPAda.

TEM revealed that the MS-ABPAda NPs had an obvious layer coating the magnetic core (Figure 1a, red arrow). Moreover, zeta potential measurements and dynamic light scattering analysis revealed that the MS-ABPAda NPs had remarkably higher zeta potentials and hydration diameters than the Fe_3O_4 NPs (43 mV vs 24 mV, Figure 1b; 37−50 nm vs 20−30 nm, Figure 1c). The magnetization curves of the Fe_3O_4 and MS-ABPAda NPs revealed that the magnetic cores had saturation magnetizations of 76 and 71 emu/g, respectively (Figure 1d), and no hysteresis loop was observed, suggesting that the NPs were superparamagnetic.

The successful modification of the MS NPs with polylysine (plys), Ada, and ABP was confirmed by quantification of the amino groups using the *N*-succinimidyl-3-(2-pyridyldithio) propionate method (Figure S3a).[46] MS had only 210 μmol of amino groups per gram, whereas MS-plys showed a much higher amino group content (850 μmol/g), which was attributed to grafting of polylysine onto the NPs. In contrast, the Ada-modified NPs, MS-plys-Ada, had an amino group content of 680 μmol/g, indicating that 20% of the amino groups on MS-plys had been modified by Ada. Grafting of ABP, which has three amino groups, onto the NPs increased the amino group content to 775 μmol/g, suggesting that 7% of the amino groups on MS-plys-Ada had been modified by ABP, and therefore, the final MS-ABPAda was successfully obtained. Thermogravimetric analysis further revealed that MS-ABPAda had more weight reduction than MS (∼32% vs ∼12%) when the temperature increased to 600 °C (Figure S3b), indicating that ∼20% organic components were grafted onto MS.

2.2. The Actin Targeting Effects of MS-ABPAda NPs. The ability of the MS-ABPAda NPs to target the actin cytoskeleton was tested in dental pulp stem cells (DPSCs), which are involved in the development of dental tissues.[47] After co-incubation with MS-ABPAda NPs, the cells were stained by the actin probe, rhodamine B-phalloidin. Confocal microscopy clearly demonstrated that the MS-ABPAda NPs (indicated by FITC) co-localized with actin, while the FITC-tagged MS-plys-Ada NPs (free of ABP) failed to target the actin (Figure S4), indicating the critical role of ABP in actin targeting. These results confirmed that the ABPAda-modified magnetic NPs were efficiently internalized, that they escaped from the endosomes (owing to the presence of positively charged polylysine), and that they specifically targeted the intracellular actin cytoskeleton.

2.3. Linear Assembly of MS-ABPAda⊂HACD Directed by an Artificial Magnetic Field. Next, to facilitate actin polarization by application of an artificial magnetic field, we designed and prepared supramolecular assemblies composed of MS-ABPAda NPs and HACD, a CD-bearing HA polymer. Dynamic light scattering analysis showed that the resulting nanocomposites were much larger and had a much broader size distribution than the MS-ABPAda NPs (250−430 nm vs 37−50 nm, Figure S5a). Moreover, the presence of negatively charged HACD on the surface of MS-ABPAda resulted in

https://dx.doi.org/10.1021/acsami.0c19428
ACS Appl. Mater. Interfaces XXXX, XXX, XXX−XXX

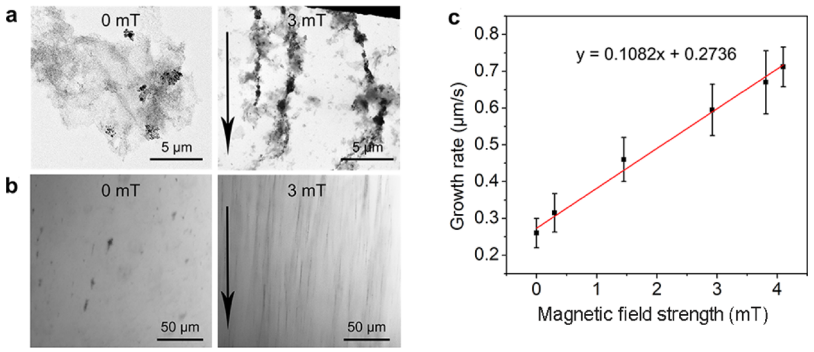

Figure 2. Formation of MS-ABPAda⊂HACD nanofibers under the influence of an artificial magnetic field. (a) TEM images of assemblies formed from MS-ABPAda NPs and HACD (100 mg/L each) in the absence and presence of an artificial magnetic field (0 and 3 mT, respectively). (b) Light microscopy images of the assemblies. (c) Relationship between the nanofiber growth rate and magnetic field strength.

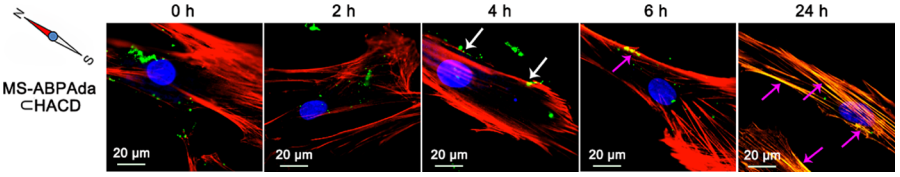

Figure 3. Internalization and intracellular assembly of MS-ABPAda⊂HACD in the DPSC cells. The confocal microscopy images indicate disassembly of the nanofibers during endocytosis (0−2 h), actin cytoskeleton targeting (4 h, indicated by the white arrows), and intracellular reassembly of the MS-ABPAda⊂HACD nanofibers at the actin cytoskeleton (6−24 h, indicated by the pink arrows) along with the direction of an artificial magnetic field (3 mT).

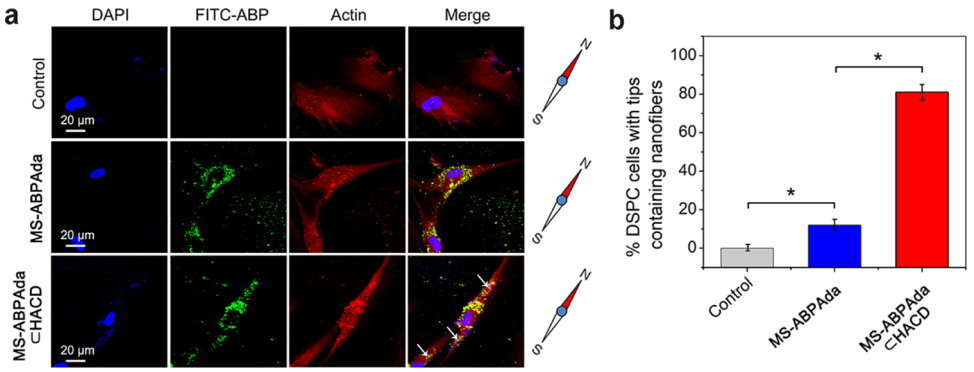

Figure 4. Induction of polarized extension of DPSCs along the direction of an artificial magnetic field (3 mT) by MS-ABPAda⊂HACD nanofibers after 24 h of incubation. (a) Confocal microscopy images of the nanofiber-treated DPSCs. The images in the columns labeled DAPI (4′,6-diamidino-2-phenylindole), FITC-ABP, and actin show the locations of the nuclei, the nanofibers, and the rhodamine B-phalloidin-stained actin cytoskeleton, respectively. The white arrows indicate nanofibers localized on the actin cytoskeleton at the DPSC extensions. (b) Percentages of DPSCs with tips containing MS-ABPAda⊂HACD nanofibers. Statistically significant differences between groups are indicated with asterisks ($P < 0.05$).

them having a zeta potential of −12 mV (vs +43 mV for the MS-ABPAda NPs, Figure S5b). The increased size and decreased zeta potential of the mixture indicated the formation of the MS-ABPAda⊂HACD supramolecular assemblies.

To determine whether these supramolecular assemblies responded to an artificial magnetic field, we monitored their formation in the absence and presence of a magnetic field by both TEM and light microscopy. When MS-ABPAda NPs and HACD were combined in the absence of a magnetic field, irregular aggregates formed (0 mT, Figure 2a,b), and the growth rate was very low (<0.3 μm/s, Figure 2c). In contrast, in the presence of a 3 mT magnetic field, the two components rapidly (within 30 s) self-assembled into long nanofibers that were aligned with the direction of the magnetic field and had diameters of 200−500 nm and lengths of 50−100 μm (Figure 2a,b). Moreover, the nanofiber growth rate increased rapidly with increasing magnetic field strength (Figure 2c). Interestingly, the relationship between growth rate and field strength was linear (Pearson correlation coefficient, 0.9966; slope, 0.1082; y-intercept, 0.2736; Figure 2c). Therefore, the MS-ABPAda⊂HACD assemblies could strongly respond to the artificial magnetic field and form nanofibers along with the direction of the magnetic field.

2.4. Application in Cell Behavior Regulation. Given that MS-ABPAda⊂HACD nanofibers are formed under the influence of a magnetic field and that the MS-ABPAda NPs could specifically target the intracellular actin cytoskeleton, we hypothesized that in mammalian cells, the nanofibers might also induce polarized organization of the intracellular actin cytoskeleton and subsequent directed extension of the cells. We tested this hypothesis by using DPSCs. Confocal microscopy was used to investigate internalization kinetics

https://dx.doi.org/10.1021/acsami.0c19428
ACS Appl. Mater. Interfaces XXXX, XXX, XXX−XXX

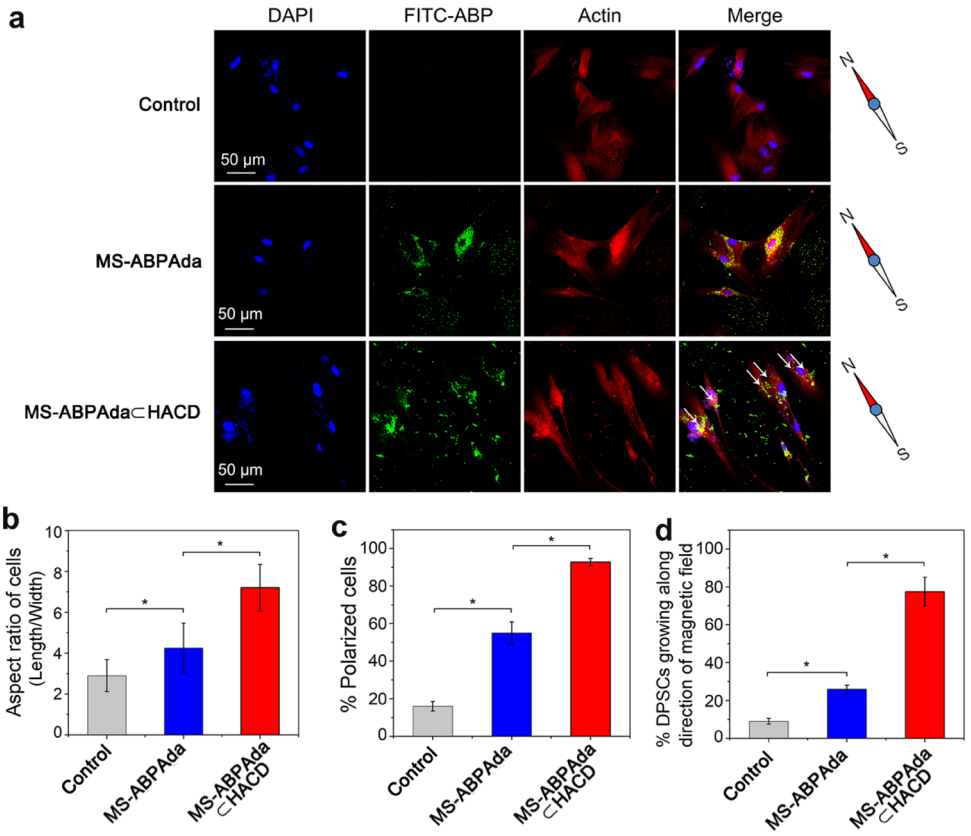

Figure 5. Magnetic field-directed polarization of DPSCs by MS-ABPAda⊂HACD nanofibers after 48 h of incubation. (a) Confocal microscopy images of control cells, MS-ABPAda-treated cells, and MS-ABPAda⊂HACD-treated cells in the presence of an artificial magnetic field (3 mT). The white arrows indicate the nanofibers localized at the actin cytoskeleton. (b) Aspect ratio of the DPSCs. (c) Percentages of polarized DPSCs (with the aspect ratio of >3.5). (d) Percentages of DPSCs growing along the direction of the magnetic field (3 mT) (with the angle between the polarization axis and the direction of the magnetic field <10°).

and intracellular assembly of the nanofibers. After the MS-ABPAda⊂HACD nanofibers contacted to the DPSCs, the nanofibers first dissembled and entered into the cells (Figure 3, 0−2 h) and then gradually targeted to the actin cytoskeleton (Figure 3, 4h, indicated by white arrows). The particle-like composites further re-assembled to form magnetic field-directed nanofibers at the cytoskeleton (Figure 3, 6−24 h, indicated by pink arrows). These observations revealed that MS-ABPAda⊂HACD could dynamically disassemble during internalization and re-assemble after targeting to the intracellular actin cytoskeleton under an artificial magnetic field.

In the process of cellular polarized growth, the cells first directedly extended along with the polarization axis in the initial short time (from 0 to 24 h) and then executed polarized growth in the following growth period (from 24 to 48 h or longer time). To investigate the effect of the supramolecular nanofibers on cellular behaviors, the DPSCs were exposed to the artificial magnetic field under the control, MS-ABPAda NP-treated or MS-ABPAda⊂HACD-treated condition, and the directed extension was first evaluated at the time point of 24 h. Under the control conditions (in the absence of the nanocomposites), the cells grew randomly in orientations on the bottom surface of the Petri dishes, and the levels of extension were low (Figure 4a, top row). The presence of MS-ABPAda NPs had no obvious impact on the direction of actin polarization or extension, even though these NPs could target the actin cytoskeleton (Figure 3a, middle row). In contrast, MS-ABPAda⊂HACD nanofibers co-located with the actin framework (indicated by the white arrows) and induced striking redirection of the actin cytoskeleton along the direction of the magnetic field after 24 h of incubation (Figure 4a, bottom row). Moreover, statistical analysis showed that a higher percentage of cells that showed tip extension had the MS-ABPAda⊂HACD nanoassemblies (Figure 4b), indicating unidirectional tip extension in the direction of the magnetic field (Figure 4a). That is, the MS-ABPAda⊂HACD nanofibers efficiently redirected actin polarization and induced directed extension of the DPSCs under the influence of an artificial magnetic field.

Directed extension of cells is frequently accompanied by cell polarized growth. Therefore, we investigated nanofiber-induced polarization of cells under a continuous long-term application of an artificial magnetic field (*i.e.*, 48 h). After this long-term treatment, the control DPSCs and DPSCs treated with MS-ABPAda NPs showed very little extension and low aspect ratios (<3 for the control cells and <5 for the NP-treated cells), and the percentages of polarized cells were also low (16 and 51%, respectively) (Figure 5a−c). These results indicate that the control cells remained in the stem cell state and that the MS-ABPAda NPs induced low-level polarization of the cells. In contrast, DPSCs treated with the MS-ABPAda HACD nanofibers showed much higher aspect ratios (~7, Figure 5a,b), and >80% of the treated cells were polarized (Figure 5c). Moreover, whereas only 8% of the control cells and 26% of the cells treated with MS-ABPAda NPs grew along the direction of the magnetic field, 80% of the nanofiber-

https://dx.doi.org/10.1021/acsami.0c19428
ACS Appl. Mater. Interfaces XXXX, XXX, XXX−XXX

treated cells showed growth in the direction of the magnetic field (Figure 5d). This directed polarization was dependent on formation of the nanofibers, as indicated by the fact that addition of an excess of the sodium salt of adamantane-1-acetic acid, which can disrupt complexation between β-CDs and Ada, to the reaction medium greatly reduced the percentage of DPSCs growing along the direction of the field (Figure S6).

Both the field strength and the concentration of the nanofibers affect cellular polarization. As the field strength increased from 0.3 to 3.81 mT, the percentage of nanofiber-treated cells growing along the direction of the field increased from 31 to 82% (Figure S7), confirming that the directed polarization of the nanofiber-treated stem cells was induced by the magnetic field. Moreover, this percent increased from 35 to 80% as the concentration of MS-ABPAda (together with HACD) increased from 25 to 100 mg/L at 3 mT (Figure S8), suggesting that the dose of the nanofibers is an important factor of cellular polarization determination.

An interesting observation is that a short time (*e.g.*, 6 h) of artificial magnetic field treatment was sufficient for inducing polarization of the nanofiber-treated DPSCs (Figure S9). While 4 h of treatment could induce 50% of polarized DPSCs, 6 h or longer time of treatment led to >70% of polarized cells (Figure S9). Furthermore, when the cells were first treated by a directed magnetic field for 24 h and then placed on another magnetic field with a changed direction, the polarized cells remained growth along with the first magnetic field direction rather than the second magnetic field direction (Figure S10), indicating that the pre-formed cellular polarization was resistant to alteration of another magnetic field. Therefore, the initial 6 h of magnetic field treatment is critical for stable polarization of the stem cells.

To verify that cell polarization depended on the actin cytoskeleton, we carried out experiments with cytochalasin D, an inhibitor of actin polymerization. As expected, when cytochalasin D was present, DPSCs treated with MS-ABPAda⊂HACD still contained nanofibers (Figure S11a), but the cells showed no extension or polarization along the direction of the magnetic field (Figure S11b,c). These results confirmed that the regulatory effects of the MS-ABPAda HACD nanofibers on DPSC polarization depended on actin polymerization, confirming that the nanofibers enhanced cell polarization by controlling directed localization of the actin cytoskeleton.

To further confirm the involvement of the MS-ABPAda⊂-HACD nanofibers in cell polarization, we evaluated their effects on the growth of another type of cells, neuron-like PC-12 cells. As was the case for DPSCs, treatment with MS-ABPAda NPs alone did not increase the aspect ratio of the PC-12 cells, and only <30% of the NP-treated cells grew along the direction of the magnetic field (Figure S12). In contrast, treatment with the MS-ABPAda⊂HACD nanofibers noticeably increased the aspect ratio, from 1.7 to 2.8 (Figure S12a,), and most of the treated cells (>70%) were polarized in the direction of the magnetic field (Figure S12a,c). Interestingly, the PC-12 exhibited less pronounced extension (Figure S12a) than DPSCs (Figure 5), which may be attributed to different cell extension properties between the two kinds of cells. Moreover, the addition of the sodium salt of adamantane-1-acetic acid (Figure S13), like the addition of cytochalasin D (Figure S14), greatly attenuated the increase in the aspect ratio and the percentage of polarized cells upon treatment with the nanofibers, verifying that both the nanofibers and the actin cytoskeleton were critical for directed polarization of the PC-12 cells.

Finally, treatment with either MS-ABPAda NPs or with the nanofibers had no obvious impact on the viability of the DPSCs or the PC-12 cells, even under the artificial magnetic field (Figure S15), implying good biocompatibility of the NPs and the nanofibers.

3. CONCLUSIONS

In summary, we constructed the supramolecular polymeric nanofibers composed of a cross-linked network of HACD polymers and magnetic NPs bearing both adamantane and ABP moieties, which are self-assembled linearly under the control of an artificial magnetic field. These host−guest nanofibers were internalized into both stem cells and targeted to the actin cytoskeleton. When the cells were treated with the nanofibers in the presence of an artificial magnetic field, directed polymerization of the actin cytoskeleton occurred, which in turn led to cellular extension and polarization along the direction of the magnetic field. Our study not only realized artificial manipulation of cell polarization by the supramolecular-based polymers but also supplied a novel strategy for remodeling cell fates distinct from traditional molecular biology methods.

4. EXPERIMENTAL SECTION

4.1. Materials. TEOS, APTES, glutaraldehyde, 1-adamantyl carboxylic acid, sodium hydroxide, EDC, NHSS, 2-morpholinoethanesulfonic acid (MES), and SPDP were purchased from Sigma, USA. Cytochalasin D, 4′,6-diamidino-2-phenylindole (DAPI), and rhodamine B-phalloidin were purchased from Thermo Fisher Scientific, USA. FITC-tagged ABP (FITC-ACP-MGVADLIKKFESISKEEC) was synthesized by Genscript, China. HACD was synthesized by the EDC/NHSS reaction between hyaluronic acid and mono-6-deoxyl-6- ethylenediamino-β-CD according to our reported method.[48,49] Other chemical reagents were purchased from Aladdin, China.

4.2. Synthesis and Characterization of the Magnetic Nanoparticles. The initial Fe_3O_4 nanoparticles were synthesized by the co-precipitation method. Briefly, 0.4 g ferrous chloride and 0.1 g ferric chloride were dissolved in 20 mL of dH_2O and then heated to 80 °C with magnetic stirring under nitrogen flux. Ammonium hydride (5 mL) (28%, w/v) were added into the solution followed by further stirring at 80 °C with magnetic stirring for 5 min. The obtained products were centrifuged and washed with dH_2O, obtaining the initial Fe_3O_4 nanoparticles.[50]

To modify the Fe_3O_4 nanoparticles with the organic molecules, 50 mg of the nanoparticles were dispersed in the mixture of 100 mg of ethanol, 25 mL of dH_2O, and 3 mL of ammonium hydroxide. TEOS (0.5 mL) was slowly added to the solution, and the mixture was stirred for 2 h. APTES (60 μL) was then added into the solution, and the mixture was further stirred for 2 h followed by centrifugation. The pellets were washed by ethanol and dH_2O and dried at room temperature, obtaining magnetic silica (MS) NPs.

MS NPs were suspended in 45 mL of dH_2O and then 5 mL of glutaraldehyde was added. The mixture was stirred at room temperature for 12 h followed by centrifugation and washing, obtaining MS-Glut. MS-Glut was responded in 50 mL of PBS and then 10 mL of PBS containing 50 mg of polylysine (M_w = 5, 000) was added into the solution. The mixture was stirred at the room temperature for 24 h and centrifuged, obtaining MS-plys.

MS-plys was further suspended in 50 mL of MES buffer (pH = 6.0, 50 mM) and then 20 mg of EDC and 22 mg of NHSS, and 20 mg of ADA were added. The mixture was stirred at room temperature for 24 h followed by centrifugation and washing, obtaining MS-plys-Ada.

MS-plys was suspended in 50 mL of DMSO and then 10 mg of SPDP and 500 μL of triethylamine (TEA) were added into the solution. The mixture was stirred at room temperature for 6 h

https://dx.doi.org/10.1021/acsami.0c19428
ACS Appl. Mater. Interfaces XXXX, XXX, XXX−XXX

followed by centrifugation and washing by DMSO and dH_2O. The pellets were further suspended in 50 mL of PBS and then 25 mg of ABP was added. The solution was stirred at 4 °C for 24 h and then the nanoparticles were harvested by centrifugation and washing, obtaining the final MS-ABPAda.

The morphology of the obtained nanoparticles was characterized by TEM (Tecnai G^2 F-20, FEI, USA), and their crystal structure and composition were determined by X-ray diffraction analysis (D/max-2500, Rigaku, Japan). The size distribution and Zeta potentials of the nanoparticles were measured using a Zeta potential analyzer (ZetaPLAS, Brookhaven, USA) at room temperature. The magnetization curves were detected using a superconducting quantum interference device (SQUID) magnetometer (MPMS7, Quantum Design, USA).

4.3. Assembly of the Nanofibers. To form the MS-ABPAda⊂HACD nanofibers, the MS-ABPAda⊂NPs and HACD were mixed in dH_2O containing 200 mg/L MS-ABPAda⊂HACD and 200 mg/L HACD. The mixture was sonicated at the room temperature for 2 min followed by rapid dropping into copper grids or confocal dishes under the artificial magnetic field with a fixed strength of 3 mT or with the indicated strengths from 0 to 3.81 mT. The assemblies were observed by TEM or by light microscopy (Zeiss, German). At each time point, the length of the nanofibers was measured, and the growth rate of the nanofibers was calculated by the length of the nanofibers at each time point divided by the assembling time. At least 50 nanofibers at each time point were measured for calculation. The correlation between the growth rate of the nanofibers and the strength of the magnetic field was analyzed by Origin software (OrigninPro 8.5, USA).

4.4. Cell Extension and Polarization Assays. The DPSCs used in this study were isolated from dental pulp of a lost tooth from healthy children, and suspended in an RPMI-1640 medium containing 10% fetal bovine serum (FBS), and cultured in a humidified incubator at 37 °C in 5% CO_2. The PC-12 neuron-like cells were obtained from the National Infrastructure of Cell Line Resource, China, and cultured in a medium containing 15% FBS.

MS-ABPAda nanoparticles (100 mg/L) or the MS-ABPAda HACD assemblies (MS-ABPAda 100 mg/L, HACD 100 mg/L, or MS-ABPAda plus HACD at the indicated equal concentrations) were added into the culture medium of the cells in confocal dishes, and the dishes were plated in the artificial magnetic field produced by NdFeB magnets. The strengths of the magnetic field were controlled by the distance between the dishes and the magnets and determined using a standard Gauss meter (Beiyi-601, Pafei, China).

To observe cellular uptake and intracellular re-assembly of the nanofibers, the DPSCs were mixed with MS-ABPAda⊂HACD (MS-ABPAda 100 mg/L, HACD 100 mg/L) in an RPMI-1640 medium containing 10% fetal bovine serum (FBS). The cells were then added into confocal dishes and placed on an artificial magnetic field (3 mT). At the indicated time points (0, 2, 4, 6, and 24 h), the cells were fixed by 4% formaldehyde for 30 min, permeabilized by 0.5% Triton X-100 solution for 10 min and then stained by the solution of rhodamine B-phalloidin (5 mg/L) and DAPI (5 mg/L) for 30 min. The cells were washed three times for observation by confocal microscopy (FV1000, Olympus, Japan).

To evaluate cell extension and polarization, the cells were treated with MS-ABPAda (100 mg/L) or MS-ABPAda⊂HACD (MS-ABPAda 100 mg/L, HACD 100 mg/L) for 24 h (evaluation of polarized extension) or 48 h (evaluation of cellular polarization) and then stained by rhodamine B-phalloidin and DAPI as described above for confocal microscope observation. The aspect ratio of the cells is defined as the length divided by the width of cells, and the polarized cells is defined as the cells with an aspect ratio of >3.5. The cells growing along with the direction of the magnetic field are defined as the cells with the angles between the polarization axis (*i.e.*, the axis linking the two extension tips of cells) and the direction of the magnetic field <10°. At least 100 cells in each group were observed for statistical analysis.

4.5. Statistical Analysis. Each experiment was performed in triplicates. The values represent the mean ± standard deviation (SD). Differences between groups were compared by one-way analysis of variance (ANOVA) test ($P < 0.05$). Statistical tests were performed using the SPSS software package (version 20, IBM).

■ ASSOCIATED CONTENT

Supporting Information

The Supporting Information is available free of charge at https://pubs.acs.org/doi/10.1021/acsami.0c19428.

Experimental procedures, detailed synthesis, cell extension and polarization assay methods, and fluorescence imaging analysis of living cell by CLSM (PDF)

■ AUTHOR INFORMATION

Corresponding Author

Yu Liu − *College of Chemistry, State Key Laboratory of Elemento-Organic Chemistry, Nankai University, Tianjin 300071, China; Collaborative Innovation Center of Chemical Science and Engineering (Tianjin), Tianjin 300072, China;* orcid.org/0000-0001-8723-1896; Email: yuliu@nankai.edu.cn

Authors

Bing Zhang − *College of Chemistry, State Key Laboratory of Elemento-Organic Chemistry, Nankai University, Tianjin 300071, China; Collaborative Innovation Center of Chemical Science and Engineering (Tianjin), Tianjin 300072, China*

Qilin Yu − *Key Laboratory of Molecular Microbiology and Technology, Ministry of Education, College of Life Sciences, Nankai University, Tianjin 300071, China;* orcid.org/0000-0003-0473-5111

Complete contact information is available at: https://pubs.acs.org/10.1021/acsami.0c19428

Author Contributions

B. Z. and Q. Y. contributes to experiment design, data acquisition, and analysis, and manuscript drafting. Y. L. contributes to conception and design of this study and critical revision of the manuscript.

Notes

The authors declare no competing financial interest.

■ ACKNOWLEDGMENTS

This work was supported by National Natural Science Foundation of China (nos. 21772099, 31870139, and 21861132001), Natural Science Foundation of Tianjin (no. 19JCZDJC33800) and China Postdoctoral Science Foundation (no. 2018 M641632).

■ ABBREVIATIONS

β-CD, *β*-cyclodextrin
HA, hyaluronic acid
HACD, *β*-CD-bearing HA polymer
Ada, adamantane
NPs, nanoparticles
MNP, magnetic NP
MS, magnetic silica
NR, nanorod
MitP, mitochondrial targeting peptide
ABP, actin-binding peptide
TEM, transmission electron microscopy
Glut, glutaraldehyde
FITC, fluorescein isothiocyanate

https://dx.doi.org/10.1021/acsami.0c19428
ACS Appl. Mater. Interfaces XXXX, XXX, XXX−XXX

ACP, aminocaproic acid

REFERENCES

(1) Chang, B.; Svoboda, K. K. H.; Liu, X. Cell Polarization: From Epithelial Cells to Odontoblasts. *Eur. J. Cell Biol.* **2019**, *98*, 1−11.

(2) Nance, J. Getting to Know Your Neighbor: Cell Polarization in Early Embryos. *J. Cell Biol.* **2014**, *206*, 823−832.

(3) Levin, M. The Embryonic Origins of Left-Right Asymmetry. *Crit. Rev. Oral Biol. Med.* **2004**, *15*, 197−206.

(4) Blanquie, O.; Bradke, F. Cytoskeleton Dynamics in Axon Regeneration. *Curr. Opin. Neurobiol.* **2018**, *51*, 60−69.

(5) Li, R.; Gundersen, G. G. Beyond Polymer Polarity: How the Cytoskeleton Builds a Polarized Cell. *Nat. Rev. Mol. Cell Biol.* **2008**, *9*, 860−873.

(6) Harris, K. P.; Tepass, U. Cdc42 and Vesicle Trafficking in Polarized Cells. *Traffic* **2010**, *11*, 1272−1279.

(7) Fietz, S. A.; Huttner, W. B. Cortical Progenitor Expansion, Self-Renewal and Neurogenesis—A Polarized Perspective. *Curr. Opin. Neurobiol.* **2011**, *21*, 23−35.

(8) Kang, H.; Jung, H. J.; Kim, S. K.; Wong, D. S. H.; Lin, S.; Li, G.; Dravid, V. P.; Bian, L. Magnetic Manipulation of Reversible Nanocaging Controls *in Vivo* Adhesion and Polarization of Macrophages. *ACS Nano* **2018**, *12*, 5978−5994.

(9) Kim, H. N.; Jang, K.-J.; Shin, J.-Y.; Kang, D.; Kim, S. M.; Koh, I.; Hong, Y.; Jang, S.; Kim, M. S.; Kim, B.-S.; Jeong, H. E.; Jeon, N. L.; Kim, P.; Suh, K.-Y. Artificial Slanted Nanocilia Array as A Mechanotransducer for Controlling Cell Polarity. *ACS Nano* **2017**, *11*, 730−741.

(10) Lomakin, A. J.; Lee, K.-C.; Han, S. J.; Bui, D. A.; Davidson, M.; Mogilner, A.; Danuser, G. Competition for Actin between Two Distinct F-actin Networks Defines a Bistable Switch for Cell Polarization. *Nat. Cell Biol.* **2015**, *17*, 1435−1445.

(11) Vidali, L.; van Gisbergen, P. A. C.; Guerin, C.; Franco, P.; Li, M.; Burkart, G. M.; Augustine, R. C.; Blanchoin, L.; Bezanilla, M. Rapid Formin-Mediated Actin-Filament Elongation is Essential for Polarized Plant Cell Growth. *Proc. Natl. Acad. Sci. U. S. A.* **2009**, *106*, 13341−13346.

(12) Li, S.; Edgar, D.; Fässler, R.; Wadsworth, W.; Yurchenco, P. D. The Role of Laminin in Embryonic Cell Polarization and Tissue Organization. *Dev. Cell* **2003**, *4*, 613−624.

(13) Riedl, J.; Crevenna, A. H.; Kessenbrock, K.; Yu, J. H.; Neukirchen, D.; Bista, M.; Bradke, F.; Jenne, D.; Holak, T. A.; Werb, Z.; Sixt, M.; Wedlich-Soldner, R. Lifeact: A Versatile Marker to Visualize F-actin. *Nat. Methods* **2008**, *5*, 605−607.

(14) Melak, M.; Plessner, M.; Grosse, R. Actin Visualization at A Glance. *J. Cell Sci.* **2017**, *130*, 525−530.

(15) Aida, T.; Meijer, E. W.; Stupp, S. I. Functional Supramolecular Polymers. *Science* **2012**, *335*, 813−817.

(16) Xing, P.; Li, P.; Chen, H.; Hao, A.; Zhao, Y. Understanding Pathway Complexity of Organic Micro/Nanofiber Growth in Hydrogen-Bonded Coassembly of Aromatic Amino Acids. *ACS Nano* **2017**, *11*, 4206−4216.

(17) Wang, K.; Wang, C.-Y.; Wang, Y.; Li, H.; Bao, C.-Y.; Liu, J.-Y.; Zhang, S. X.-A.; Yang, Y.-W. Electrospun Nanofibers and Multi-Responsive Supramolecular Assemblies Constructed from A Pillar[5]-arene-Based Receptor. *Chem. Commun.* **2013**, *49*, 10528−10530.

(18) Ma, X.; Tian, H. Stimuli-Responsive Supramolecular Polymers in Aqueous Solution. *Acc. Chem. Res.* **2009**, *47*, 1971−1981.

(19) Sun, C.; Wang, Z.; Yue, L.; Huang, Q.; Cheng, Q.; Wang, R. Supramolecular Induction of Mitochondrial Aggregation and Fusion. *J. Am. Chem. Soc.* **2020**, *142*, 16523−16527.

(20) Su, Y. S.; Liu, J. W.; Jiang, Y.; Chen, C. F. Assembly of A Self-Complementary Monomer: Formation of Supramolecular Polymer Networks and Responsive Gels. *Chemistry* **2011**, *17*, 2435−2441.

(21) Chen, H.; Ma, X.; Wu, S.; Tian, H. A Rapidly Self-Healing Supramolecular Polymer Hydrogel with Photostimulated Room-Temperature Phosphorescence Responsiveness. *Angew. Chem., Int. Ed.* **2014**, *53*, 14149−14152.

(22) Wang, Q.; Chen, Y.; Liu, Y. Supramolecular Ternary Polymer Mediated by Cucurbituril and Cyclodextrin. *Polym. Chem.* **2013**, *4*, 4192−4198.

(23) Harada, A.; Takashima, Y.; Nakahata, M. Supramolecular Polymeric Materials via Cyclodextrin−Guest Interactions. *Acc. Chem. Res.* **2014**, *47*, 2128−2140.

(24) Gu, W.-X.; Li, Q.-L.; Lu, H.; Fang, L.; Chen, Q.; Yang, Y. W.; Gao, H. Construction of Stable Polymeric Vesicles Based on Azobenzene and Beta-cyclodextrin Grafted Poly(glycerol methacrylate)s for Potential Applications in Colon-specific Drug Delivery. *Chem. Commun.* **2015**, *51*, 4715−4718.

(25) Yu, Q.; Zhang, Y.-M.; Liu, Y.-H.; Xu, X.; Liu, Y. Magnetism and Photo Dual-controlled Supramolecular Assembly for Suppression of Tumor Invasion and Metastasis. *Sci. Adv.* **2018**, *4*, eaat2297.

(26) Zhou, J.; Li, J.; Du, X.; Xu, B. Supramolecular Biofunctional Materials. *Biomaterials* **2017**, *129*, 1−27.

(27) Ang, C.-Y.; Tan, S. Y.; Wang, X.; Zhang, Q.; Khan, M.; Bai, L.; Tamil Selvan, S.; Ma, X.; Zhu, L.; Nguyen, K. T.; Tan, N. S.; Zhao, Y. Supramolecular Nanoparticle Carriers Self-assembled from Cyclodextrin- and Adamantane-functionalized Polyacrylates for Tumor-targeted Drug Delivery. *J. Mater. Chem. B* **2019**, *2*, 1879−1890.

(28) Quan, C.-Y.; Chen, J.-X.; Wang, H.-Y.; Li, C.; Chang, C.; Zhang, X.-Z.; Zhuo, R.-X. Core-shell nanosized assemblies mediated by the alpha-beta cyclodextrin dimer with a tumor-triggered targeting property. *ACS Nano* **2010**, *4*, 4211−4219.

(29) Zhang, J.; Ma, P. X. Cyclodextrin-based Supramolecular Systems for Drug Delivery: Recent Progress and Future Perspective. *Adv. Drug Delivery Rev.* **2013**, *65*, 1215−1233.

(30) Thatiparti, T. R.; Shoffstall, A. J.; Von Recum, H. A. Cyclodextrin-Based Device Coatings for Affinity-based Release of Antibiotics. *Biomaterials* **2010**, *31*, 2335−2347.

(31) Liang, W.; Huang, Y.; Lu, D.; Ma, X.; Gong, T.; Cui, X.; Yu, B.; Yang, C.; Dong, C.; Shuang, C. β-Cyclodextrin−Hyaluronic Acid Polymer Functionalized Magnetic Graphene Oxide Nanocomposites for Targeted Photo-Chemotherapy of Tumor Cells. *Polymer* **2019**, *11*, 133.

(32) Kayaci, F.; Umu, O. C. O.; Tekinay, T.; Uyar, T. Antibacterial Electrospun Poly(lactic acid) (PLA) Nanofibrous Webs Incorporating Triclosan/Cyclodextrin Inclusion Complexes. *J. Agric. Food Chem.* **2013**, *61*, 3901−3908.

(33) Li, X.; Bai, H.; Yang, Y.; Yoon, J.; Wang, S.; Zhang, X. Supramolecular Antibacterial Materials for Combatting Antibiotic Resistance. *Adv. Mater.* **2019**, *31*, 1805092.

(34) Thatiparti, T. R.; von Recum, H. A. Cyclodextrin Complexation for Affinity-Based Antibiotic Delivery. *Macromol. Biosci.* **2010**, *10*, 82−90.

(35) Li, Y.; Zhang, C.; Zhou, Y.; Dong, Y.; Chen, W. Novel Multi-Responsive Polymer Materials: When Ionic Liquids Step in. *Eur. Polym. J.* **2015**, *69*, 441−448.

(36) Xu, H.; Cui, L.; Tong, N.; Gu, H. Development of High Magnetization Fe_3O_4/Polystyrene/Silica Nanospheres via Combined Miniemulsion/Emulsion Polymerization. *J. Am. Chem. Soc.* **2006**, *128*, 15582−15583.

(37) Du, L.; Xu, Z.-Y.; Fan, C.-J.; Xiang, G.; Yang, K.-K.; Wang, Y.-Z. A Fascinating Metallo-supramolecular Polymer Network with Thermal/Magnetic/Light-responsive Shape-memory Effects Anchored by Fe_3O_4 Nanoparticles. *Macromolecules* **2018**, *51*, 705−715.

(38) Lee, J. H.; Chen, K. J.; Noh, S. H.; Garcia, M. A.; Wang, H.; Lin, W. Y.; Jeong, H.; Kong, B. J.; Stout, D. B.; Cheon, J.; Tseng, H. R. On-demand Drug Release System for in vivo Cancer Treatment through Self-assembled Magnetic Nanoparticles. *Angew. Chem. Int. Edit.* **2013**, *52*, 4384−4388.

(39) Kumar, C. S. S. R.; Mohammad, F. Magnetic Nanomaterials for Hyperthermia-based Therapy and Controlled Drug Delivery. *Adv. Drug Delivery Rev.* **2011**, *63*, 789−808.

(40) Kang, H.; Kim, S.; Wong, D. S. H.; Jung, H. J.; Lin, S.; Zou, K.; Li, R.; Li, G.; Dravid, V. P.; Bian, L. Remote Manipulation of Ligand Nano-Oscillations Regulates Adhesion and Polarization of Macrophages in vivo. *Nano Lett.* **2017**, *17*, 6415−6427.

https://dx.doi.org/10.1021/acsami.0c19428
ACS Appl. Mater. Interfaces XXXX, XXX, XXX−XXX

(41) Hoffmann, C.; Mazari, E.; Lallet, S.; Le Borgne, R.; Marchi, V.; Gosse, C.; Gueroui, Z. Spatiotemporal Control of Microtubule Nucleation and Assembly Using Magnetic Nanoparticles. *Nat. Nanotechnol.* **2013**, *8*, 199−205.
(42) Wang, Z.; Qin, W.; Zhuang, J.; Wu, M.; Li, Q.; Fan, C.; Zhang, Y. Virus-Mimicking Cell Capture Using Heterovalency Magnetic DNA Nanoclaws. *ACS Appl. Mater. Interfaces* **2019**, *11*, 12244−12252.
(43) Yu, Q.; Zhang, Y. M.; Liu, Y. H.; Liu, Y. Magnetic Supramolecular Nanofibers of Gold Nanorods for Photothermal Therapy. *Adv. Therap.* **2019**, *2*, 1800137.
(44) Guo, X.; Farías, G. G.; Mattera, R.; Bonifacino, J. S. Rab5 and Its Effector FHF Contribute to Neuronal Polarity through Dynein-dependent Retrieval of Somatodendritic Proteins from the Axon. *Proc. Natl. Acad. Sci. U. S. A.* **2016**, *113*, E5318−E5327.
(45) Conforti, P.; Besusso, D.; Bocchi, V. D.; Faedo, A.; Cesana, E.; Rossetti, G.; Ranzani, V.; Svendsen, C. N.; Thompson, L. M.; Toselli, M.; Biella, G.; Pagani, M.; Cattaneo, E. Faulty Neuronal Determination and Cell Polarization are Reverted by Modulating HD Early Phenotypes. *Proc. Natl. Acad. Sci. U. S. A.* **2018**, *115*, E762−E771.
(46) Moser, M.; Nirmalananthan, N.; Behnke, T.; Geißler, D.; Resch-Genger, U. Multimodal Cleavable Reporters versus Conventional Labels for Optical Quantification of Accessible Amino and Carboxy Groups on Nano- and Microparticles. *Anal. Chem.* **2018**, *90*, 5887−5895.
(47) Yu, Q.; Li, J.; Zhang, Y.; Wang, Y.; Liu, L.; Li, M. Inhibition of Gold Nanoparticles (AuNPs) on Pathogenic Biofilm Formation and Invasion to Host Cells. *Sci. Rep.* **2016**, *6*, 26667.
(48) Yang, Y.; Zhang, Y.-M.; Chen, Y.; Chen, J.-T.; Liu, Y. Targeted Polysaccharide Nanoparticle for Adamplatin Prodrug Delivery. *J. Med. Chem.* **2013**, *56*, 9725−9736.
(49) Li, N.; Chen, Y.; Zhang, Y. M.; Yang, Y.; Su, Y.; Chen, J. T.; Liu, Y. Polysaccharide-gold Nanocluster Supramolecular Conjugates as A Versatile Platform for the Targeted Delivery of Anticancer Drugs. *Sci. Rep.* **2014**, *4*, 4164.
(50) Zhu, N.; Zhang, B.; Yu, Q. Genetic Engineering-Facilitated Coassembly of Synthetic Bacterial Cells and Magnetic Nanoparticles for Efficient Heavy Metal Removal. *ACS Appl. Mater. Interfaces* **2020**, *12*, 22948−22957.

https://dx.doi.org/10.1021/acsami.0c19428
ACS Appl. Mater. Interfaces XXXX, XXX, XXX−XXX